(Received 25 July 2025, Accepted 16 September 2025, Scheduled 25 September 2025)

Highly-Miniaturized Broadband MIMO Antennas for WLAN/WiMAX/5G and UWB Communications

Lubab A. Salman* and Kareem Madhloom Gatea

Department of Electronic and Communications Engineering, College of Engineering, Al-Nahrain University, Baghdad 64040, Iraq

ABSTRACT: Highly-miniaturized MIMO antennas are very much desired for 5G-and-beyond hand-held devices as well as miniaturized stationary devices for WSN and IoT applications. In this paper, two compact two-port printed MIMO arrays, measuring $28\times14\times0.8\,\text{mm}^3$ each, with and without isolation enhancement, are proposed. These arrays have nearly omnidirectional radiation patterns over an extended operational bandwidth. The proposed designs feature an extended set of control parameters by which the desired performance could be achieved without compromising space and weight requirements or accuracy. They were fine tuned to provide an operational bandwidth about 4 GHz with relatively low starting frequencies of 2.7 and 3.3 GHz, respectively, allowing simultaneous WiFi, WiMax, 5G operation with a moderate gain and very high efficiency. Prototypes are manufactured and examined for impedance bandwidth, isolation, diversity, and radiation properties showing very good agreement with simulation results.

1. INTRODUCTION

Printed antennas, along with complementary microwave structures and radio frequency (RF) electronics, form the cornerstone of the ongoing revolution in wireless communications. One key approach gaining importance in enhancing wireless systems involves utilizing diversity techniques to mitigate the impact of the harsh communication environment on system reliability. Spatial, polarization, and radiation pattern diversity techniques are techniques that involve implementing specially designed antennas and/or antenna arrays. These techniques use variably placed antenna elements with diverse radiation characteristics to provide the system with a mix of signal samples from the rich scattering environment for further processing. Multiple-input multiple-output (MIMO) systems involve arrays of equally-spaced identical antenna elements on both sides of the communications link to help, along with appropriate MIMO encoding/decoding techniques, achieving this goal.

MIMO systems rely on the presence of multiple induction and sampling elements on both ends of the communication link. They also assume that the elements on each side are identical and equally spaced with a minimum separation of $\lambda/2$, ensuring that the field magnitude remains unaffected by the design or placement of any individual source or solicitor. Under these conditions, only linear phase variation is experienced by the individual array elements as a plane electromagnetic wave is passing by. When these criteria are met, signal strength fluctuations and nonlinear phase variations are controlled solely by the baseband system to improve performance. Thus, miniaturized arrays with closely spaced MIMO elements need to maintain large isolation so as to sustain performance optimization.

Several miniaturized broadband two-port MIMO antenna designs with good or high isolation have been proposed in the literature. Some have incorporated some isolation enhancement mechanism [1–8]; others have relied on the individual element design or inter-element spacing to reduce coupling [5, 9, 10].

A critical challenge in modern wireless devices is the stringent limitation on physical size, which constrains the allowable dimensions of onboard RF electronics and microwave components. The key limiting factor in such assemblies is the antenna elements and their arrays. Many researchers have explored compact MIMO antenna designs [1–39], but achieving wideband operation (more than 20% bandwidth) and high isolation with two-port configurations of very small form factors remains challenging.

To systematically evaluate the progress in this domain, two critical design metrics emerge: *antenna footprint* and *antenna impedance bandwidth per unit volume*. Antenna **footprint** refers to the total area occupied by a printed antenna. This directly determines the antenna's integration feasibility in space-constrained devices like smartphones or IoT modules. Within the above analyzed literature, its value was found between $279\,\text{mm}^2$ and $7150\,\text{mm}^2$. The **fractional impedance bandwidth per unit volume (FIB/V)**, on the other hand, is defined here to quantify how efficiently a given design is capable of distilling operational bandwidth into a unit volume. The value of FIB/V was found well below $0.2\%\,\text{mm}^{-3}$ for most of the models proposed in the analyzed literature, but no more than $0.3\%\,\text{mm}^{-3}$ for the other cases which will be considered next.

Several relatively small (800–$1200\,\text{mm}^2$) [19, 20, 24, 26–28, 38], and even very compact (400–$800\,\text{mm}^2$) [1–3, 5, 8], designs have been reported in the literature. Many of them, however, exhibit either large volumes or narrow operational bandwidths, resulting in very low FIB/V values — well below

* Corresponding author: Lubab A. Salman (lubab.ali.1@nahrainuniv.edu.iq).

$0.1\%\,\mathrm{mm}^{-3}$. In contrast, some designs within the same footprint range have managed to achieve higher FIB/V by realizing reduced volumes and/or broader bandwidths [4, 6, 32]. For example, Alharbi et al. [4] reduced their design volume to $512\,\mathrm{mm}^3$, resulting in an improved FIB/V of approximately $0.16\%\,\mathrm{mm}^{-3}$ for a footprint of $640\,\mathrm{mm}^2$, albeit with a more modest bandwidth of 81.1%. Using a circular arch patch with a partial ground plane, Urimubenshi et al. [6] achieved a wider impedance bandwidth of 100% within a relatively small volume of $678\,\mathrm{mm}^3$, resulting in a FIB/V of about $0.15\%\,\mathrm{mm}^{-3}$ and a footprint of $424\,\mathrm{mm}^2$. Notably, Khedr et al. [32] attained an FIB/V of approximately $0.17\%\,\mathrm{mm}^{-3}$ at a larger footprint of $1700\,\mathrm{mm}^2$ solely by increasing the operational bandwidth to 162%.

Other designs have demonstrated even higher FIB/V values — exceeding $0.2\%\,\mathrm{mm}^{-3}$ [7, 25, 31]. For instance, You et al. [31] achieved an impressive FIB/V of approximately $0.3\%\,\mathrm{mm}^{-3}$ by employing a very thin substrate (0.1 mm), albeit with a relatively modest bandwidth of 50% and at the expense of a large footprint ($1680\,\mathrm{mm}^2$). In comparison, Chaudhary and Manohar [25] and Wu et al. [7] realized FIB/V values of $0.22\%\,\mathrm{mm}^{-3}$ and $0.25\%\,\mathrm{mm}^{-3}$ at smaller footprints of $822.5\,\mathrm{mm}^2$ and $567\,\mathrm{mm}^2$, respectively, benefiting from significantly broader bandwidths of approximately 178% and 114%. These results illustrate that simultaneously achieving both a small footprint and a large fractional bandwidth per unit volume remains a highly challenging and often conflicting design objective.

It is also noteworthy that some compact designs face significant limitations despite their promising dimensions. For instance, although Yang et al. [12] achieved a minimal footprint of $279\,\mathrm{mm}^2$, the design's bandwidth remains quite narrow, and with a substrate thickness of 1.6 mm, the resulting FIB/V is not superior to $0.3\%\,\mathrm{mm}^{-3}$. Moreover, the maximum simulated gain is only 0.72 dBi, which significantly restricts its suitability for long-range wireless communication scenarios. Another interesting case is the two-port, geometrically symmetrical, high-isolation MIMO antenna proposed by Beigi et al. [40]. While this design offers the advantages of a low-cost FR-4 substrate (1 mm thick), a very compact footprint ($10 \times 20\,\mathrm{mm}^2$), and exceptionally high isolation (not less than 30 dB), it fails to function as a true diversity antenna because of a mismatch in the impedance bandwidth (IBW) between its two elements. This limitation persists despite the overall geometrical symmetry of the antenna, including its isolation electromagnetic band gap (EBG) structure, which would ideally ensure identical frequency responses for both elements!

Building on these observations, this work introduces a flexible design framework featuring a comprehensive set of control parameters that facilitate seamless integration with other RF components and enable precise tuning to meet specific operational requirements. The proposed antenna design addresses the aforementioned challenges by placing two identical, highly miniaturized antenna elements in close proximity, complemented by a straightforward inter-element structure to enhance isolation. Despite its compact form factor, the MIMO array achieves a wide impedance bandwidth and maintains relatively high isolation, operating effectively within the sub-6 GHz band and covering the entire NR FR-1 spectrum above 3.3 GHz. Furthermore, it supports high data rate communications through UWB techniques, making the array well-suited for a broad range of wireless communication protocols with MIMO capability and allowing simultaneous multi-standard operation.

The remainder of this paper is organized as follows. Section 2 presents and discusses in detail the key development steps leading to the realization of final MIMO antennas. Simulation and measurement results, along with diversity performance metrics, are thoroughly analyzed in Section 3. In Section 4, the achievements of this work are compared with closely related studies in the literature. Finally, Section 5 concludes the paper.

2. ANTENNA DESIGN

The antenna design process underwent several development cycles, comprising five main steps as illustrated in Fig. 1:

1. Development of a compact annular monopole antenna intended to cover the S and C bands, with the lowest possible lower cutoff frequency (**Antenna 1**).
2. Enhancement of Antenna 1's performance by extending the ground plane with a T-shaped branch, consisting of a duplicated ground plane positioned at the top of the structure and connected via a vertical strip (**Antenna 2**).
3. Duplication of Antenna 2 to realize a two-port MIMO antenna, doubling the overall width compared to a single antenna (**Antenna 3**).
4. Introduction of a vertical strip at the center of the ground plane to improve the isolation between ports (**Antenna 4**).
5. Addition of square side notches at the feed ends of both annular patches to further fine-tune the lower and upper cutoff frequencies of the antenna's impedance bandwidth (**Antenna 5** and **Antenna 6**).

Throughout all development cycles, the substrate material was chosen as low-cost FR-4 with $\epsilon_r = 4.3$ and $\tan\delta = 0.025$. The substrate thickness is going to be determined after evaluating its impact on the antenna's impedance bandwidth.

In the following sections, we examine the key performance characteristics of each design iteration in the frequency domain to evaluate the impact of each control parameter on the final antenna design. All simulations are conducted using Computer Simulation Technology (CST) Microwave Studio® 2025.

2.1. The Annular Monopole Antenna

The single element of the proposed MIMO design (Antenna 1) is a compact annular monopole, well known for its broadband and omnidirectional characteristics. It is adopted with slight modifications based on the initial development steps presented in [6] and [41]. Due to its planar configuration, the inner and outer radii of the annular patch have a less pronounced effect than its overall area and average radius on the antenna's performance. The annular patch area and its average (or center)

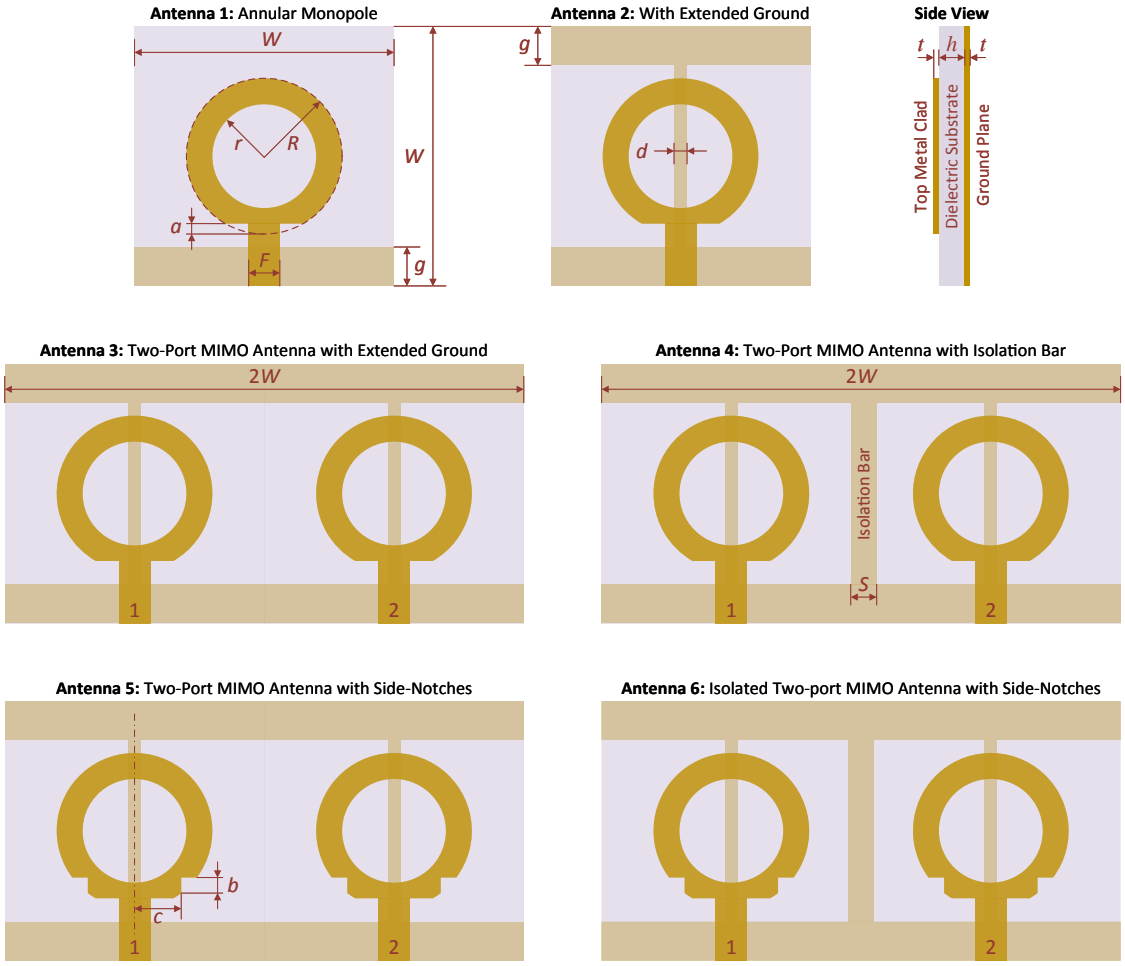

FIGURE 1. Development cycles of the proposed compact two-port MIMO antenna.

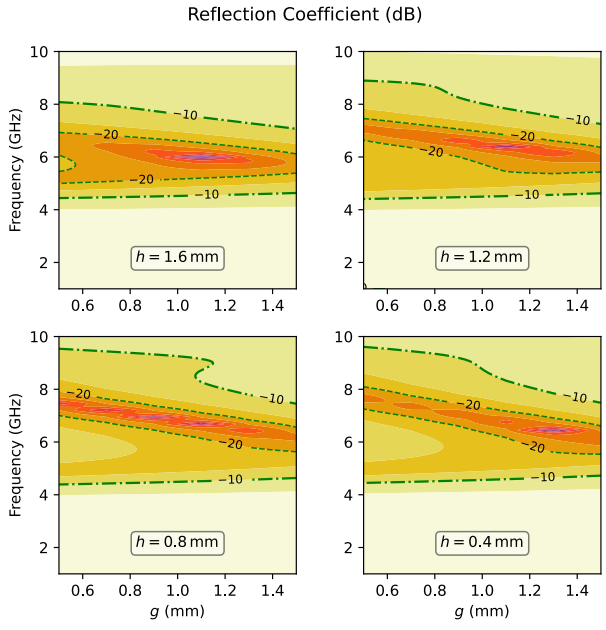

FIGURE 2. The impedance bandwidth response of the annular monopole (Antenna 1) to varying substrate thickness with fixed patch area ($A_p = 40\,\text{mm}^2$) and average patch radius ($r_c = 4\,\text{mm}$). The substrate material is FR-4 with $\epsilon_r = 4.3$, $\tan\delta = 0.025$.

radius, denoted as A_p and r_c, respectively, are related to the inner and outer radii, r and R, by the following expressions:

$$A_p = \pi(R^2 - r^2) \tag{1}$$

$$r_c = \frac{R + r}{2} \tag{2}$$

Figure 2 illustrates the variation of impedance bandwidth with the ground plane height g — which defines the feed gap (the distance between the upper ground edge and the patch) — for different substrate thicknesses. In all cases, the feed-line width F is adjusted to maintain a $50\,\Omega$ microstrip line impedance. Correspondingly, the patch feed trim a is fine-tuned to ensure a smooth transition between the feedline and the patch. It is observed that a broader matching bandwidth can be achieved by reducing the substrate thickness to $h = 0.8\,\text{mm}$. Further reduction to $0.4\,\text{mm}$, however, leads to a decrease in the matching bandwidth as a function of frequency and ground plane height. To maximize FIB/V in the final design while preserving parametric flexibility, a substrate thickness of $0.8\,\text{mm}$ is selected for all subsequent development cycles.

Figure 3 illustrates the effect of patch dimensions on the frequency response of the annular monopole antenna. It is evident that increasing the patch size — whether by area or average radius — generally leads to a reduction in the available

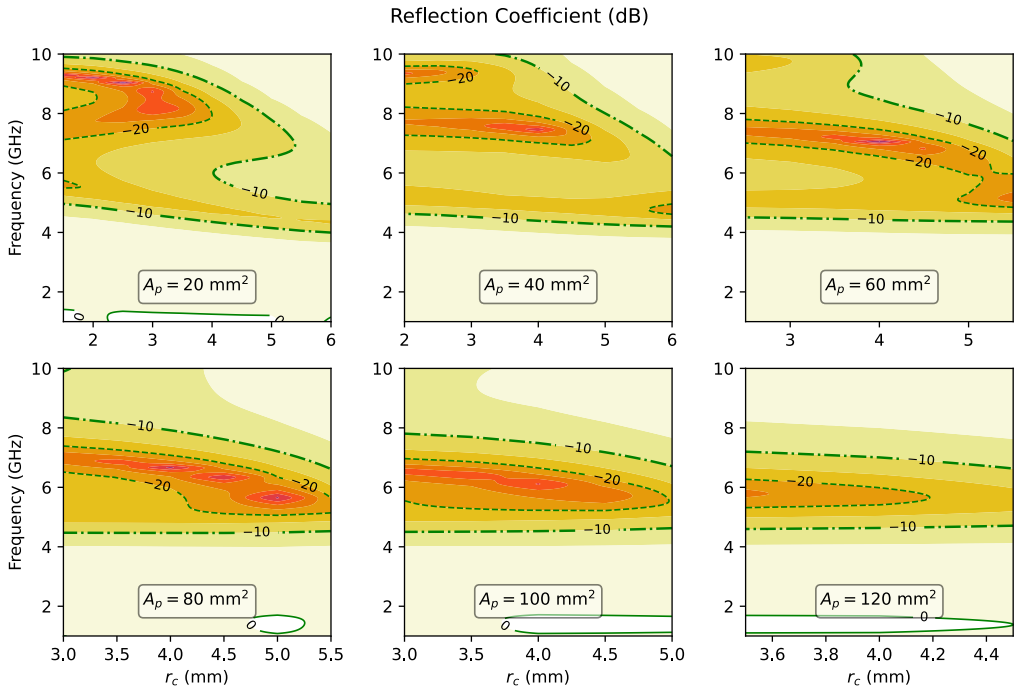

FIGURE 3. The impact of patch area and average patch radius on monopole impedance bandwidth for a ground height of 0.5 mm. The patch trim at the feedline end varies between 0.1 and 0.3 mm to ensure seamless feedline to patch transition.

impedance bandwidth. Optimal performance, characterized by the greatest bandwidth, is observed for a patch area of approximately 40 mm^2 and an average radius below 4 mm. However, these results are preliminary, as placing two antenna elements side by side is expected to influence their individual responses.

2.2. A Single Monopole with Extended Ground Plane

Despite the respectable impedance bandwidth of approximately 5 GHz offered by the annular monopole antenna (Antenna 1) across a wide range of ground plane heights with a substrate thickness of 0.8 mm, the lower cutoff frequency remains insufficient to cover WiMAX as well as lower-frequency WiFi and 5G-NR bands. To address this, a T-shaped extension is introduced in the ground plane, as shown for Antenna 2 in Fig. 1. This modification results in a noticeable reduction of the lower cutoff frequency, albeit at the expense of a narrower total bandwidth, as illustrated for selected parameter sets (A_p, r_c, g) in Fig. 4. Start frequencies as low as 3.6 GHz are now attainable, compared to a minimum of 4.3 GHz without the ground plane extension. Further improvements in this performance are observed when incorporating this monopole element into the MIMO design.

2.3. Two-Port MIMO Antenna

Placing two annular monopoles with extended ground planes side-by-side results in a MIMO configuration suitable for 2×2 wireless MIMO communications. This design, shown in Fig. 1 as Antenna 3, is further analyzed in Fig. 5, which illustrates the impact of selected parameter combinations on antenna performance. It is evident that the impedance bandwidth can be significantly increased, with the lower cutoff frequency extending well below 3 GHz across a wide range of geometric configurations. A respectable operational bandwidth is achievable for numerous parameter sets, all featuring a relatively low starting frequency. The accompanying transmission coefficient plots indicate that an isolation exceeding 20 dB is attainable only over a limited portion of the frequency range within these bands; however, an acceptable isolation of approximately 10 dB is maintained throughout the operational bandwidth.

To further enhance isolation, a vertical strip — hereafter referred to as isolation bar — is introduced in the ground plane at the junction between the two antenna elements, connecting the upper and lower sections (Antenna 4 in Fig. 1). Fig. 6 demonstrates an improvement of approximately 5 dB in isolation compared to the configuration without the isolation bar shown in Fig. 5. This enhancement, however, comes at the expense of a slight reduction in impedance bandwidth. In the final designs, two side notches are incorporated into the patch near the feedline to provide additional control over the antenna response without increasing the footprint or compromising the FIB/V, as detailed in the following section.

2.4. The Proposed MIMO Designs

Antenna 5 and Antenna 6 represent two versions of the proposed compact two-port MIMO antenna — one without isolation enhancement and the other incorporating it. In both designs, side notches are introduced on either side of the feedline in the patch to provide additional control over the antenna's impedance bandwidth. An analysis of Figs. 5 and 6 indicates that excellent performance — characterized by wide impedance bandwidth, low startup frequency, and acceptable isolation — can be achieved with parameters approximately set

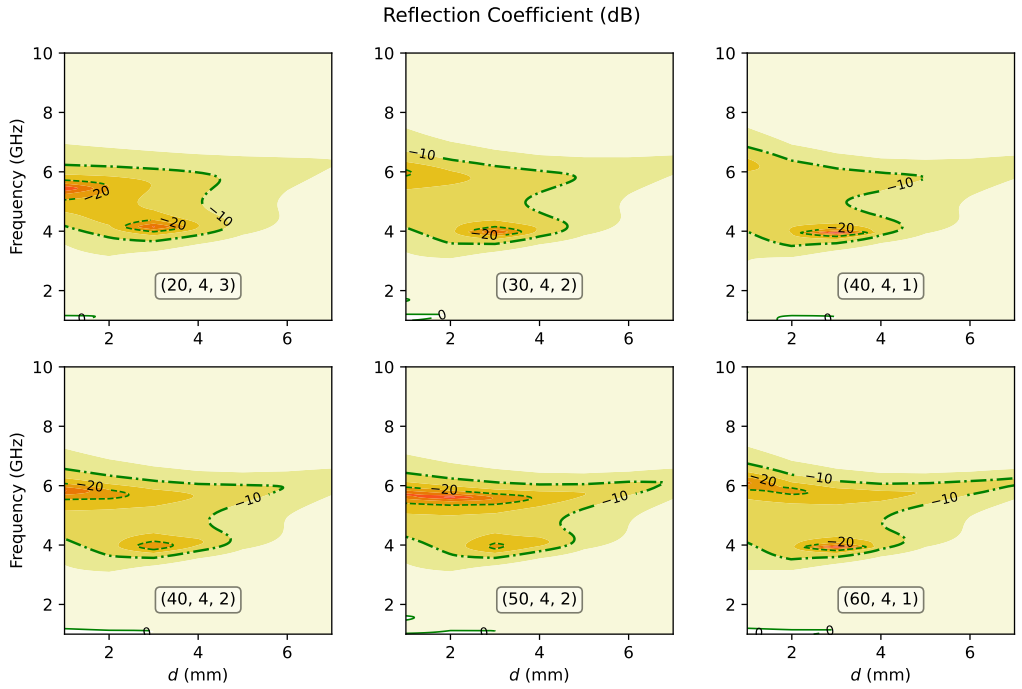

FIGURE 4. The response of Antenna 2 to various patch areas, average patch radii, and ground heights as a function of the ground strip width in the frequency domain. The tuple in each slide indicates the values of A_p (mm^2), r_c (mm), and g (mm), respectively.

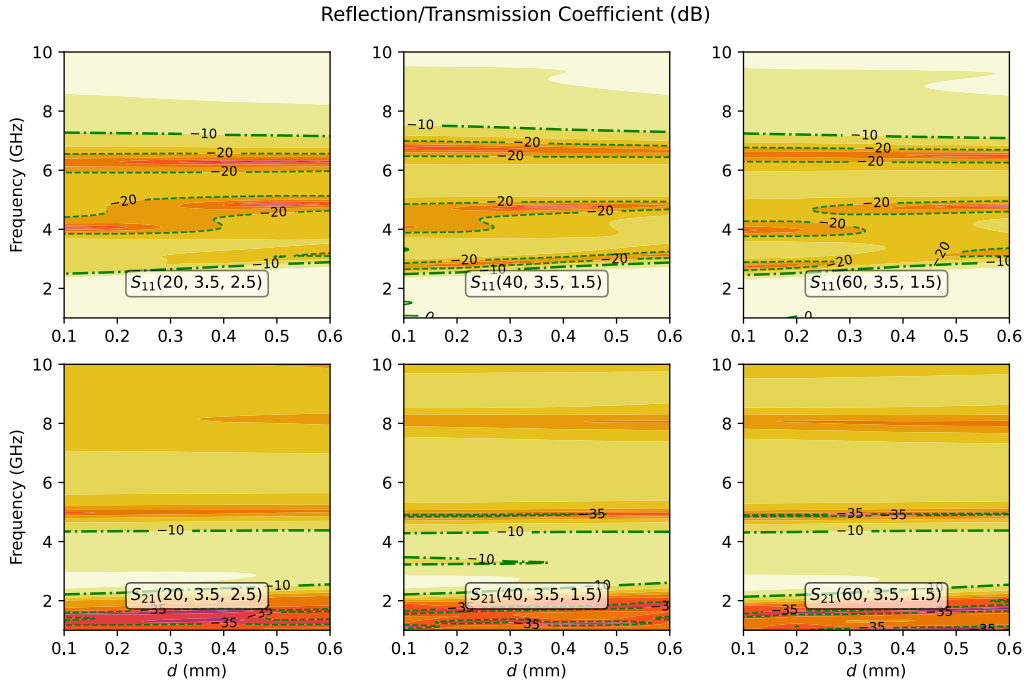

FIGURE 5. The response of Antenna 3 to various patch areas, average patch radii, and ground heights as a function of the ground strip width in the frequency domain. The tuple in each slide indicates the values of A_p (mm^2), r_c (mm), and g (mm), respectively.

to $A_p = 40\,\text{mm}^2$, $r_c = 3.5\,\text{mm}$, $g = 2\,\text{mm}$, $d = 0.3\,\text{mm}$, and $S = 1.5\,\text{mm}$ in the isolation-enhanced design. Fixing these values and selecting notch dimensions $b = c = 0.5\,\text{mm}$ for both versions result in the reflection and transmission coefficients depicted in Fig. 7. It is evident that the two designs exhibit nearly identical impedance bandwidths of approximately 4.6 GHz, differing mainly in startup frequency, while the isolation-enhanced design shows a significant improvement in isolation across the operating band.

From the foregoing investigation, it is clear that the proposed designs provide a comprehensive set of control parameters, allowing flexible tuning of their frequency-domain performance. To enable simultaneous operation of multiple wireless communication protocols, these parameters can be further optimized.

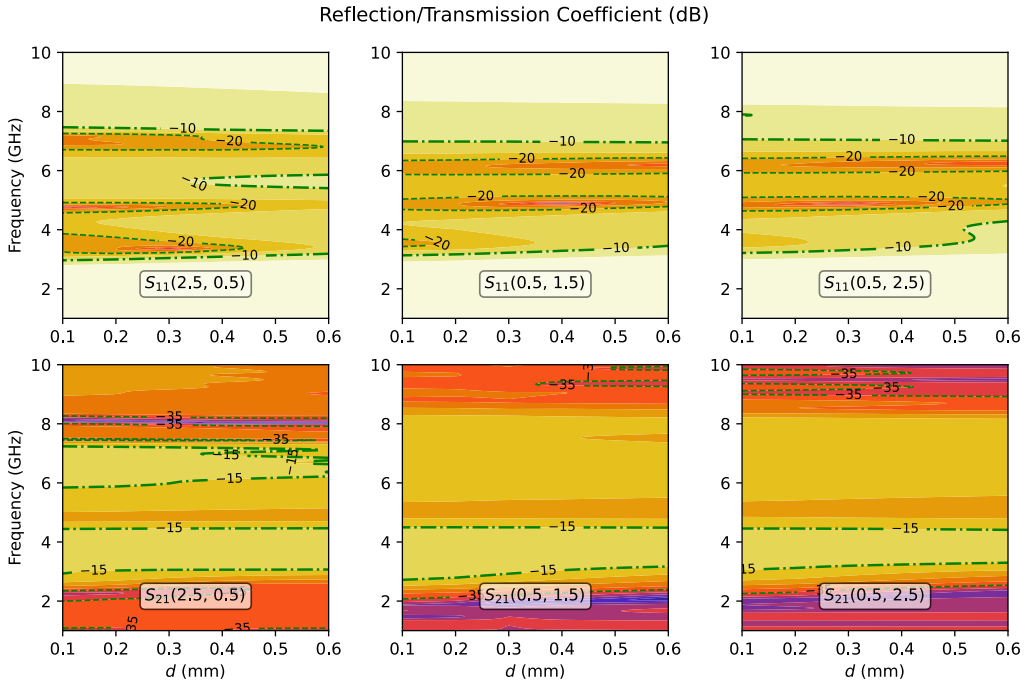

FIGURE 6. The response of Antenna 4 to various patch areas, average patch radii, and ground heights as a function of the ground strip width in the frequency domain for $A_p = 40\,\text{mm}^2$ and $r_c = 3.5\,\text{mm}$. The tuple in each slide indicates the values of g (mm) and S (mm), respectively.

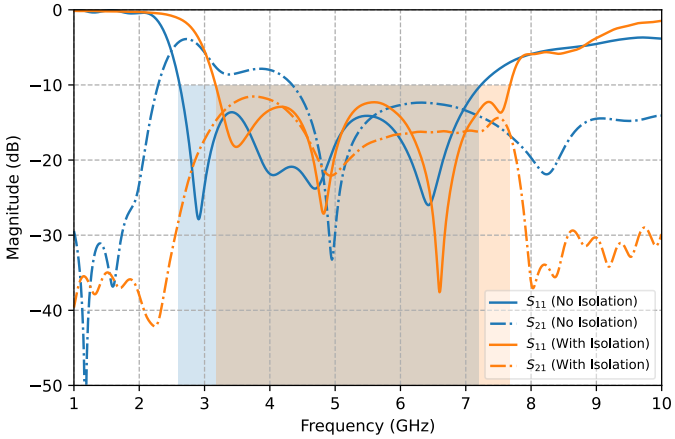

FIGURE 7. The frequency responses of Antenna 5 and Antenna 6 for $A_p = 40\,\text{mm}^2$, $r_c = 3.5\,\text{mm}$, $a = 0.1\,\text{mm}$, $g = 2\,\text{mm}$, $d = 0.3\,\text{mm}$, $S = 1.5\,\text{mm}$, $b = 0.5\,\text{mm}$, and $c = 0.5\,\text{mm}$.

The next section presents and discusses the diversity performance and radiation characteristics of the proposed designs for two refined parameter sets, aimed at facilitating coverage of the wireless communication protocols illustrated in Fig. 8.

3. RESULTS AND DISCUSSION

Two sets of geometric design parameters are selected for the final experimental validation of the two proposed MIMO designs — with and without isolation enhancement. The parameter values are listed in Tables 1 and 2, respectively. The corresponding simulated and fabricated models, along with the S-parameter measurement setup, are shown in Figs. 9 and 10, respectively.

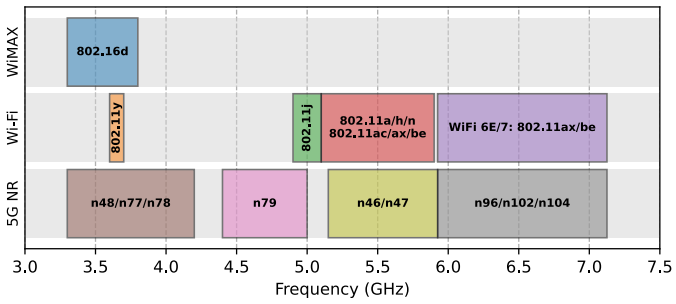

FIGURE 8. Wireless communication protocols and the bands they occupy in the 3 to 7.5 GHz frequency range.

3.1. Impedance Bandwidth and Mutual Coupling

Simulated and measured results for the final designs are presented in Figs. 11 and 12. As shown in Fig. 11, the reflection coefficients (S_{11} and S_{22} in dB) of the fabricated prototypes achieve the desired impedance bandwidth, effectively covering the operational bands illustrated in Fig. 8. The transmission coefficients (S_{21} and S_{12} in dB) closely match the simulation predictions. Notably, the isolation exceeds 10 dB only at frequencies above 4.5 GHz within the target band, while it ranges between 4 and 8 dB at lower frequencies. The enhanced isolation model exhibits a significant improvement of approximately 5 dB, as shown in Fig. 12. However, this gain in isolation comes at the cost of reduced bandwidth, reflected by a slight increase in the lower cutoff frequency in simulations and a more pronounced shift in the measured prototype. This discrepancy is attributed to the antenna's miniaturization, which reduces its dimensions to a scale comparable to the feeding SMA connectors and soldering paste, making the antenna highly sensitive to minor fabrication variations from the simulation model.

TABLE 1. Geometrical parameters of the proposed MIMO design without isolation enhancement.

Parameter	W	R	r	a	b	c	d	g
Value (mm)	14	4.4	2.8	0.3	0.5	0.4	0.3	2.2

TABLE 2. Geometrical parameters of the proposed MIMO design with isolation enhancement.

Parameter	W	R	r	a	b	c	d	g	S
Value (mm)	14	4.6	2.5	0.2	0.5	1.1	0.2	2	1.4

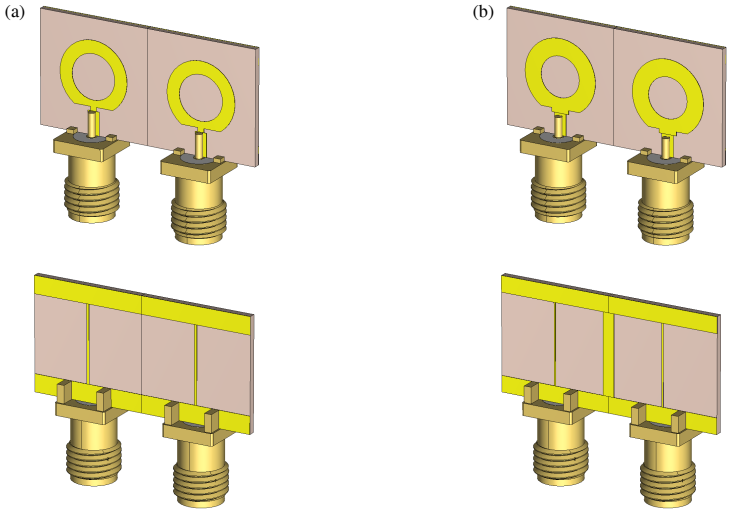

FIGURE 9. Simulation models of the proposed compact two-port MIMO antennas. (a) Without isolation bar. (b) With isolation bar.

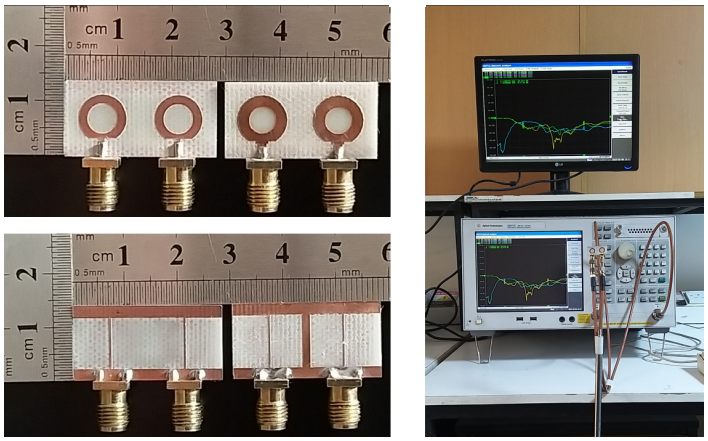

FIGURE 10. Prototypes of the porposed MIMO antenna designs with and without isolation enhancement, with the S-parameters measurement setup.

Figure 13 illustrates the effect of the isolation bar on the average power flow within the antenna structure when port 1 is excited at selected operational frequencies. It is evident that, in the absence of the isolation bar, more power is coupled to port 2, whereas the presence of the isolation bar significantly reduces this coupling. This effect becomes increasingly pronounced at higher frequencies, consistent with the transmission coefficient results shown in Figs. 11 and 12.

3.2. Diversity Analysis

MIMO communication systems require good isolation between antenna elements, typically achieved by maintaining an inter-element spacing at least $\lambda/2$ at the operating frequency. However, this approach often leads to physically large antenna arrays, especially at lower frequencies. To ensure acceptable system performance, the diversity behavior of MIMO antenna arrays is commonly characterized using specific diversity met-

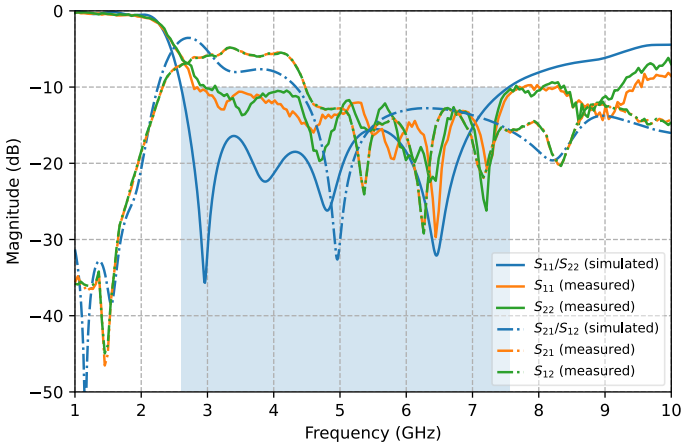

FIGURE 11. Reflection and transmission coefficients of the proposed compact two-port MIMO antenna without isolation.

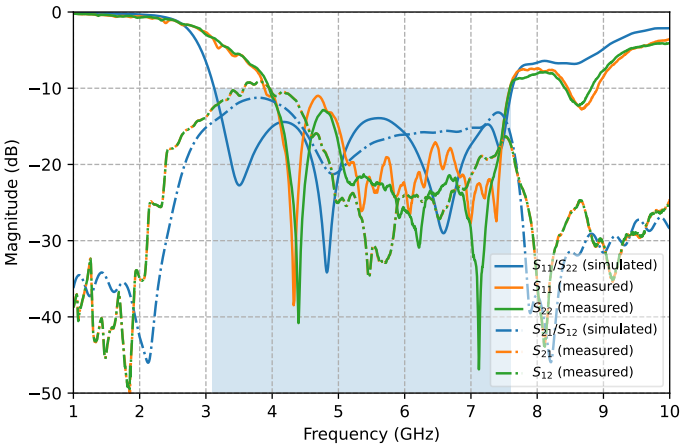

FIGURE 12. Reflection and transmission coefficients of the proposed compact two-port MIMO antenna with isolation bar.

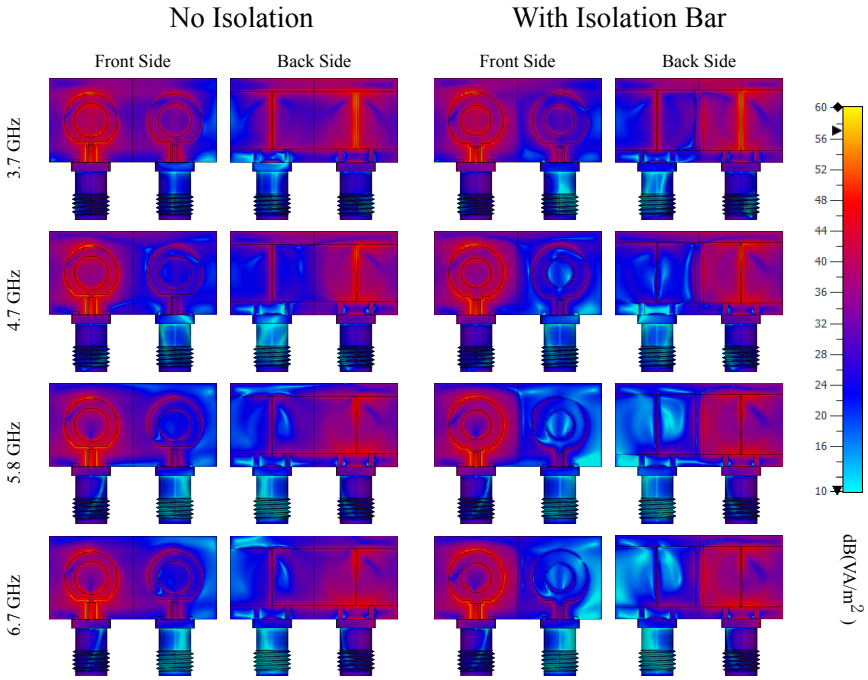

FIGURE 13. Average power density flow with port 1 excited at selected operating frequencies.

rics. These metrics assess the design's ability to exploit diversity mechanisms to enhance communication performance, without relying solely on inter-element spacing. They are generally derived from the antenna array's radiation characteristics, either predicted theoretically or obtained from measurements. Importantly, these diversity metrics can often be expressed in terms of the array's scattering parameters (S-parameters).

In particular, the reflection coefficient measures the ability of a single antenna element in a wireless communication link to accept RF power from a source or deliver it to subsequent stages with minimal backscattering. However, for a MIMO array, the performance of individual elements does not directly represent the overall capacity of the entire array. Therefore, the total active reflection coefficient (TARC) is used to assess the array's performance as a whole. TARC is defined as the square root of the ratio of the total power reflected by the RF-driven array to the total power supplied, and is mathematically expressed as:

$$\text{TARC} = \frac{\sqrt{\sum_{i=1}^{N} |b_i|^2}}{\sqrt{\sum_{i=1}^{N} |a_i|^2}} \tag{3}$$

where a_i and b_i respectively represent the incident and scattered waves at each of the N ports of the MIMO array. For the two-element arrays proposed in this paper, this ratio is simplified to

$$\text{TARC} = \frac{\sqrt{|S_{11} + S_{12}|^2 + |S_{21} + S_{22}|^2}}{\sqrt{2}} \tag{4}$$

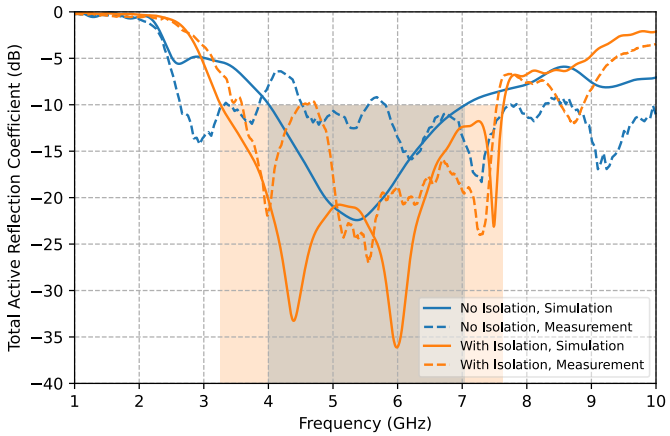

FIGURE 14. Total active reflection coefficient of the proposed compact two-port MIMO antennas, with and without isolation.

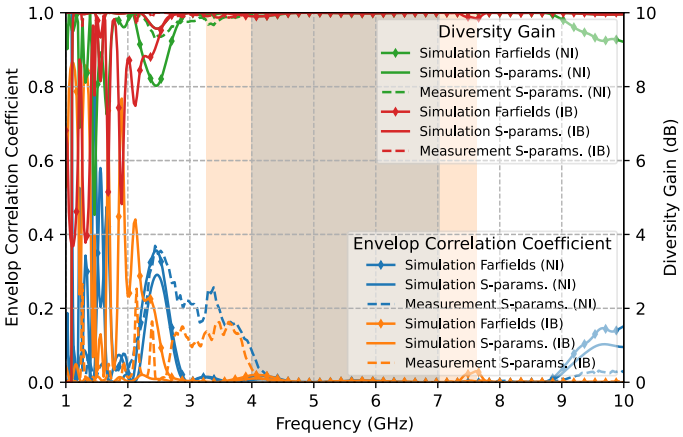

FIGURE 15. Envelop correlation coefficient and diversity gain of the proposed compact two-port MIMO antennas, with isolation bar (IB) and with no isolation (NI).

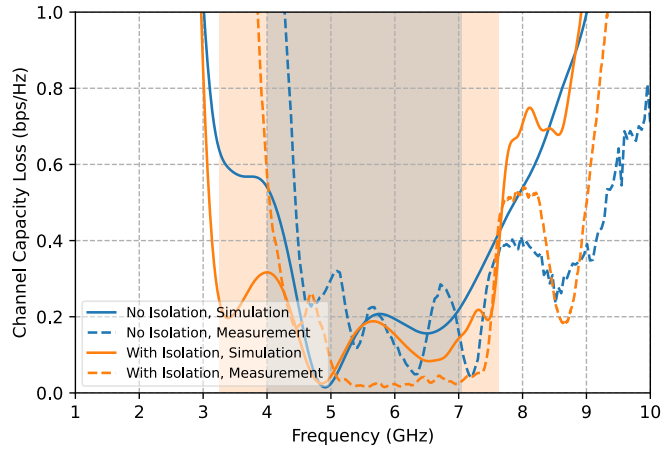

FIGURE 16. Channel capacity loss of the proposed compact two-port MIMO antennas, with and without isolation.

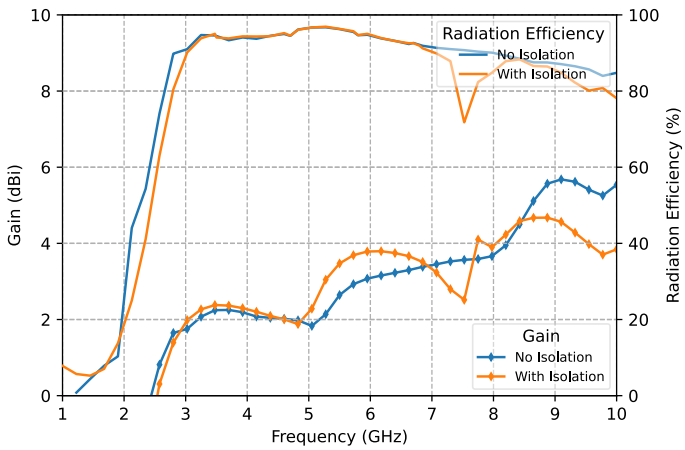

FIGURE 17. Simulated gain and radiation efficiency for the proposed antennas, with and without isolation.

in terms of the system's scattering parameters, assuming that the two ports are simultaneously fed in-phase. Using this equation along with the previously obtained simulation and measurement results for the two final MIMO antenna designs, the system TARC is calculated and presented in Fig. 14 in dB. It is evident that incorporating the isolation bar in the final design significantly improves the TARC bandwidth. Specifically, the design without isolation enhancement exhibits a considerably narrower TARC bandwidth, insufficient to reliably support MIMO operation for the targeted wireless communication protocols in a rich scattering environment. The other diversity metrics will be examined within the confines of these two bands for the final MIMO arrays.

Three additional parameters are crucial in evaluating the performance of MIMO antenna arrays. The envelope correlation coefficient (ECC) quantifies the level of interdependence between individual MIMO communication channels. This correlation depends on the actual radiation patterns of the antenna elements as well as the symmetry of the scattering environment in which the array operates. For a MIMO array of two elements, it is given by

$$\rho_e = \frac{\left|\sum_{p,q}\int_\Omega E_{1p}(\Omega)E^*_{2q}(\Omega)P_{pq}(\Omega)\,d\Omega\right|^2}{\prod_{m=1}^{2}\sum_p\int_\Omega |E_{mp}(\Omega)|^2 P_{pp}(\Omega)\,d\Omega} \tag{5}$$

where $p, q = [\theta, \phi]$; Ω is the solid angle of the integral domain; and P_{pq} are the elements of the polarization matrix of waves impinging on the antenna from all directions [42]. For balanced scattering environments and identical radiation patterns, the polarization matrix becomes an identity, and ECC can be expressed in terms of system's scattering parameters as follows [43]:

$$\rho_e = \frac{\left|S^*_{11}S_{12} + S^*_{21}S_{22}\right|^2}{\left(1-|S_{11}|^2-|S_{21}|^2\right)\left(1-|S_{22}|^2-|S_{12}|^2\right)} \tag{6}$$

Using Eqs. (5) and (6), ECC is calculated from simulation and measurement results and presented in Fig. 15 for both designs, with and without isolation enhancement. Near-zero correlation is observed within the -10 dB TARC bands identified from the

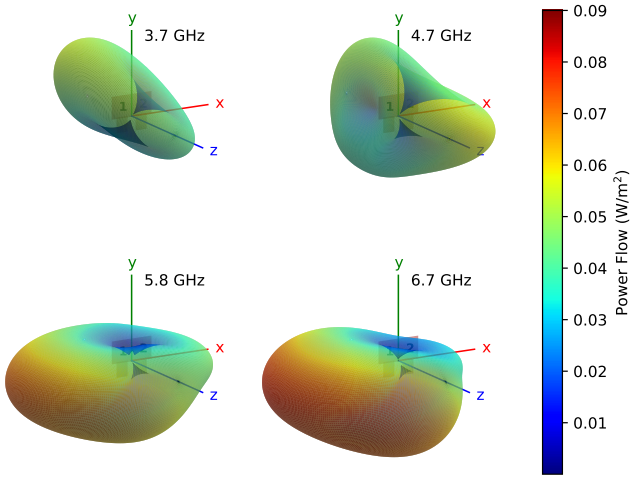

FIGURE 18. 3D radiation pattern at four select frequencies for the proposed design without isolation enhancement when Element 1 is excited.

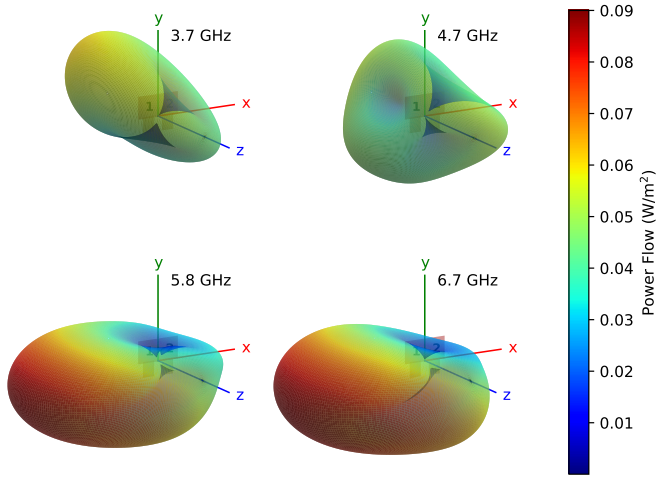

FIGURE 19. 3D radiation pattern at four selected frequencies for the proposed design with isolation enhancement when Element 1 is excited.

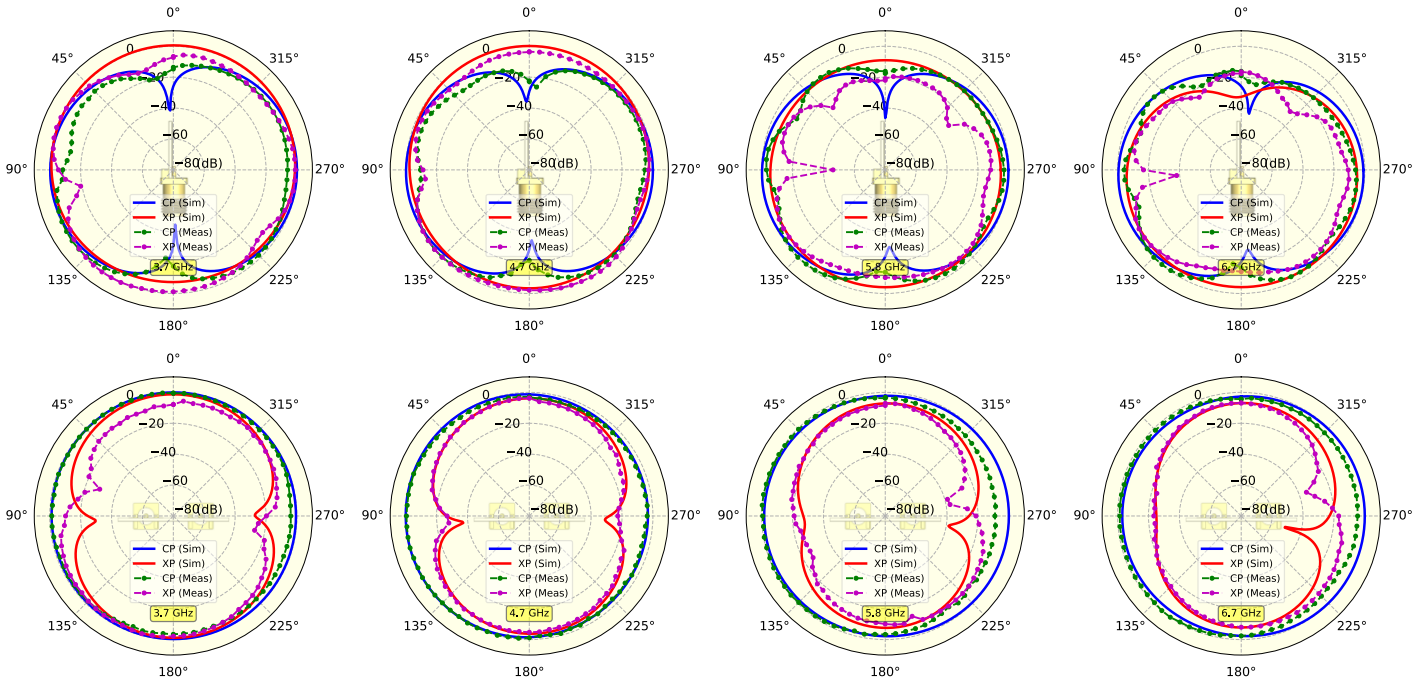

FIGURE 20. Simulated (Sim) and measured (Meas) normalized E-plane (top row) and H-plane (bottom row) radiation patterns for the proposed antenna without an isolation structure. (CP: Copolar, XP: Crosspolar).

simulations for both designs. Similar performance is seen in the measurements, with only slight and acceptable deviations at lower frequencies attributed to manufacturing tolerances.

In contrast to ECC, diversity gain (DG) quantifies the independence of individual MIMO channels rather than their interdependence. Accordingly, DG is inversely related to ECC and can be approximated in dB for two-port MIMO antennas using the following formula:

$$\mathrm{DG} = 10\sqrt{1 - |\rho_e|^2} \tag{7}$$

The corresponding results are also shown in Fig. 15, clearly demonstrating excellent performance across the entire band of interest for both designs.

Finally, the impact of the antenna performance on system capacity can be evaluated by calculating the capacity loss at different frequencies, which is given by

$$\mathrm{CCL} = -\log_2 \det\left(\mathbf{I} - \mathbf{S}^{\dagger}\mathbf{S}\right) \tag{8}$$

in terms of the system's scattering parameters, where $\mathbf{S}$ represents the scattering matrix. Fig. 16 shows that the design with isolation enhancement incurs an acceptable capacity loss of less than 0.3 bps/Hz within the targeted frequency band, although some discrepancies are observed between simulation and measurement-based CCL calculations.

Considering this set of diversity measures, it is clear that the proposed compact MIMO designs achieve satisfactory diver-

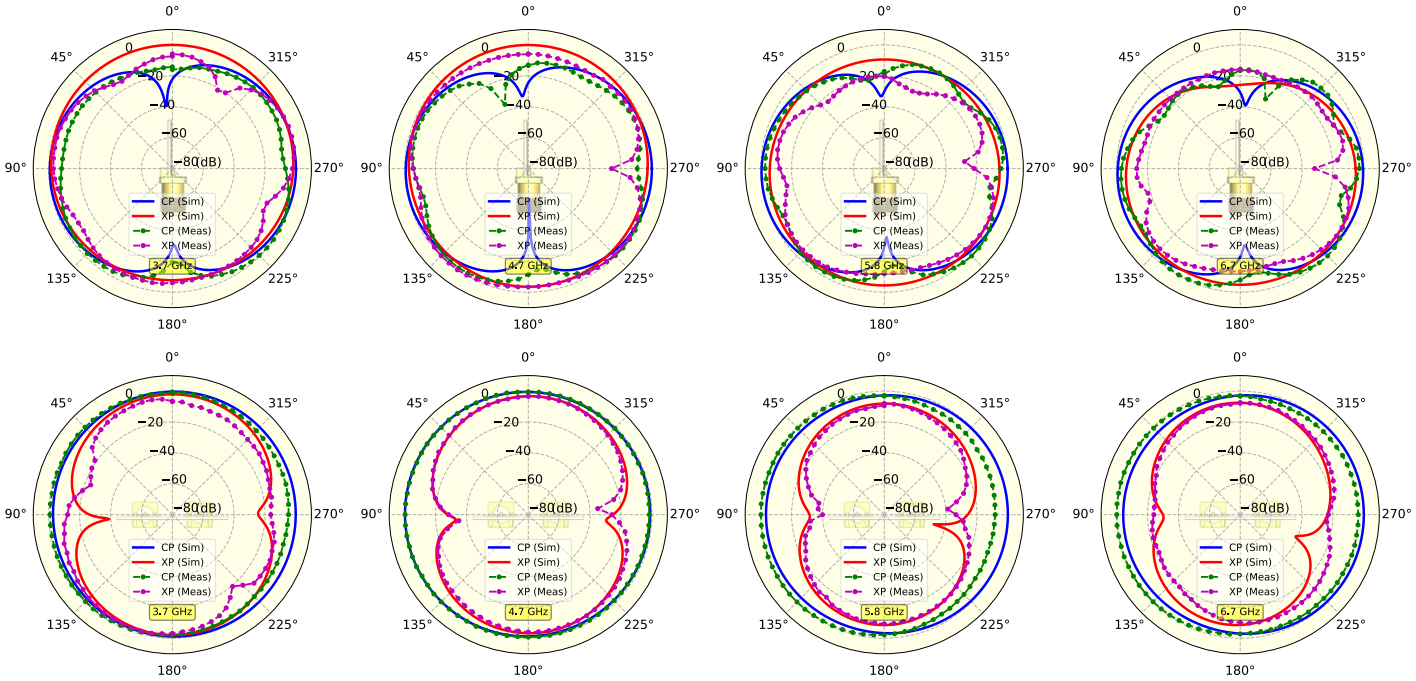

FIGURE 21. Simulated (Sim) and measured (Meas) normalized E-plane (top row) and H-plane (bottom row) radiation pattern for the proposed antenna with an isolation bar. (CP: Copolar, XP: Crosspolar).

sity performance over the desired frequency band, particularly for the design with isolation enhancement.

3.3. Radiation Characteristics

In addition to wide impedance bandwidth and good isolation performance, the proposed designs exhibit excellent radiation efficiency and considerable gain in the H-plane, owing to their nearly omnidirectional radiation pattern, as shown in Fig. 17. Radiation efficiency exceeds 90% within the band of interest, while the gain increases with frequency from approximately 2 dBi to nearly 4 dBi across the band. Interestingly, the introduction of the isolation bar appears to have a positive impact on antenna gain, particularly at higher frequencies within the targeted range.

To further investigate radiation characteristics of the two proposed designs, their 3D radiation patterns at four selected frequencies are presented in Figs. 18 and 19. Both figures are drawn to scale, clearly illustrating the gain enhancement associated with the introduction of the isolation bar at higher frequencies.

To verify the accuracy of the estimations, co- and cross-polarized radiation patterns in the E- and H-planes were measured and compared to the corresponding simulation results, as shown in Figs. 20 and 21. Apart from inevitable measurement errors, the measured patterns closely replicate the simulated ones with a high degree of accuracy. Both E- and H-plane results clearly reflect the omnidirectional nature of the proposed designs, making them excellent candidates for applications where the orientation of the wireless link is not predetermined. The corresponding measurement setup is shown in Fig. 22, where the antenna under test (AUT) is illuminated by a

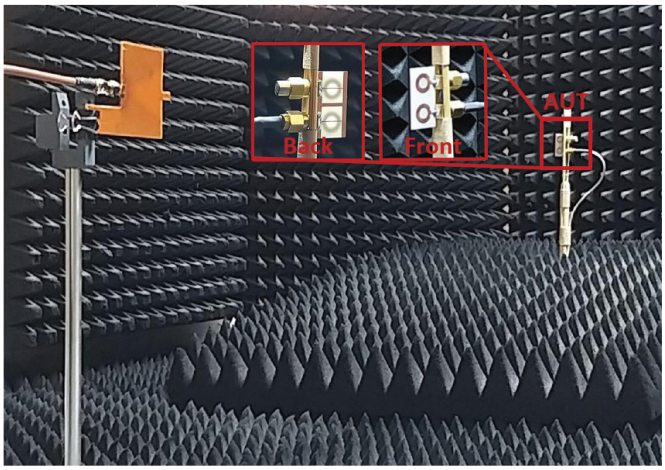

FIGURE 22. Radiation pattern measurement. (The antenna under test (proposed) is in receiving mode, and the source antenna is wide-band, high-gain, and low cross-polarization antenna fabricated in compliance with the suggestions in [44] and [45].)

custom-made antenna featuring a very high cross-polarization discrimination ratio [44, 45].

4. CONSTRUCTION AND PERFORMANCE GAINS

The proposed two-port MIMO antenna designs offer simplicity, low cost, and a rich set of control parameters, enabling the easy derivation of multiple optimized parameter sets to meet diverse performance requirements. The straightforward annular patch structure, combined with side notches, facilitates variation of the patch area and curvature to satisfy various impedance and

TABLE 3. Comparison with closely related recent literature.

Reference	Footprint (mm^2)	Thickness (mm)	f_L (GHz)	f_H (GHz)	FIB (%)	FIB/V (%mm^{-3})	Isolation (dB)	Gain (dBi)
[31]	**1680**	0.1	3	5	50	**0.298**	20	2
[32]	1170	0.8	2.3	21.7	161.7	0.173	10.29	19.91
[38]	900	1.6	2.74	14.8	137.5	0.095	20	5.4
[25]	**822.5**	1	1.78	30	177.6	**0.216**	22	6.6
[4]	640	0.8	3.3	7.8	81.1	0.158	20	3
[5] — First Design	600	1.6	4.27	10.1	81.1	0.085	20	2.75-6
[5] — Second Design	600	1.6	4.27	10.1	81.1	0.085	52	3-7
[3]	570	0.8	3.1	4.37	34	0.075	18	1.2-2.91
[7]	**567**	0.8	3	11	114.3	**0.252**	15	2.5
[6]	423.8	1.6	4	12	100	0.147	15	5.57
This Work (No Isolation)	**392**	0.8	2.7	7.4	93.1	**0.297**	7.5	2-4
This Work (With Isolation)	**392**	0.8	3.3	7.6	78.9	**0.252**	11.2	2-4

radiation specifications. The symmetrical ground plane cuts allow tuning of the lower cutoff frequency and bandwidth without significantly affecting the antenna's radiation characteristics. Similar benefits apply to the isolation bar, which provides improved isolation. Diversity metrics demonstrate excellent performance within the frequency range of interest, with high radiation efficiency and respectable gain considering the design's simplicity. These achievements are further highlighted and compared to recent state-of-the-art designs reported in the literature, as summarized in Table 3.

5. CONCLUSION

This paper has presented two compact two-port MIMO antenna designs tailored for modern wireless communication systems, with and without isolation enhancement. Through systematic design evolution, the introduction of an isolation bar in the ground plane has been demonstrated to significantly improve isolation — by approximately 5 dB — while maintaining a favorable impedance bandwidth. The incorporation of side notches and symmetrical ground plane cuts provides a versatile set of design parameters, enabling flexible tuning of impedance bandwidth, radiation characteristics, and lower cutoff frequency without compromising the antenna's footprint or performance.

Extensive simulation and measurement results confirm that both designs achieve wide impedance bandwidth, excellent radiation efficiency exceeding 90%, and nearly omnidirectional radiation patterns suitable for applications with variable link orientation. The enhanced isolation design further exhibits superior diversity performance, as evidenced by key metrics such as envelope correlation coefficient (ECC), diversity gain (DG), total active reflection coefficient (TARC), and channel capacity loss (CCL). These metrics collectively indicate reliable MIMO operation across targeted wireless communication bands, outperforming many recent comparable designs reported in the literature.

The positive impact of the isolation bar on antenna gain at higher frequencies, along with the robust antenna miniaturization strategies employed, highlights the practical applicability of the proposed designs for compact, high-performance MIMO arrays. Overall, the proposed antennas offer a compelling balance among simplicity, size, and multi-parameter optimization capability, making them strong candidates for the integration into next-generation wireless devices that demand compactness and high diversity performance.

Future work could extend this design approach to multi-element MIMO configurations and explore advanced isolation enhancement techniques to further improve system capacity and reliability in increasingly complex communication environments.

ACKNOWLEDGEMENT

The authors sincerely thank the Department of Electronic and Communications Engineering at the College of Engineering, Al-Nahrain University, for providing the tools and equipment essential for conducting the frequency domain and radiation pattern measurements.

REFERENCES

[1] Pouyanfar, N., C. Ghobadi, J. Nourinia, K. Pedram, and M. Majidzadeh, "A compact multi-band MIMO antenna with high isolation for C and X bands using defected ground structure," *Radioengineering*, Vol. 27, No. 3, 686–693, 2018.

[2] Kumar, J. P. and G. Karunakar, "Compact C-shaped MIMO diversity antenna for quad band applications with hexagonal stub for isolation improvement," *International Journal of RF and Microwave Computer-Aided Engineering*, Vol. 29, No. 12, e21971, 2019.

[3] Kumar, A., A. Q. Ansari, B. K. Kanaujia, J. Kishor, and S. Kumar, "An ultra-compact two-port UWB-MIMO antenna with dual band-notched characteristics," *AEU — International Journal of Electronics and Communications*, Vol. 114, 152997, 2020.

[4] Alharbi, A. G., J. Kulkarni, A. Desai, C.-Y.-D. Sim, and A. Poddar, "A multi-slot two-antenna MIMO with high isolation for sub-6 GHz 5G/IEEE802. 11ac/ax/C-band/X-band wireless and satellite applications," *Electronics*, Vol. 11, No. 3, 473, 2022.

[5] Kumar, P., R. Sinha, A. Choubey, and S. K. Mahto, "DGS based miniaturized wideband MIMO antenna with efficient isolation for C band applications," *Frequenz*, Vol. 77, No. 3-4, 163–172, 2023.

[6] Urimubenshi, F., D. B. O. Konditi, J. d. Dieu Iyakaremye, P. M. Mpele, and A. Munyaneza, "A novel approach for low mutual coupling and ultra-compact Two Port MIMO antenna development for UWB wireless application," *Heliyon*, Vol. 8, No. 3, e09057, 2022.

[7] Wu, L., X. Cao, and B. Yang, "Design and analysis of a compact UWB-MIMO antenna with four notched bands," *Progress In Electromagnetics Research M*, Vol. 108, 127–137, 2022.

[8] Godi, R. C. and R. R. Patil, "SRA-DGS-NL based decoupling scheme for MIMO antenna," *Progress In Electromagnetics Research C*, Vol. 148, 1–7, 2024.

[9] Sanugomula, M. and K. K. Naik, "A compact high gain circular shaped two-port MIMO antenna with fractal DGS for downlink satellite communication," *Progress In Electromagnetics Research M*, Vol. 125, 135–142, 2024.

[10] Sanugomula, M. and K. K. Naik, "Design of a CSRR dual-port patch antenna with elliptical slots on ground plane for wireless communication," *Progress In Electromagnetics Research C*, Vol. 143, 151–160, 2024.

[11] Sharawi, M. S., A. B. Numan, and D. N. Aloi, "Isolation improvement in a dual-band dual-element MIMO antenna system using capacitively loaded loops," *Progress In Electromagnetics Research*, Vol. 134, 247–266, 2013.

[12] Yang, L., T. Li, and S. Yan, "Highly compact MIMO antenna system for LTE/ISM applications," *International Journal of Antennas and Propagation*, Vol. 2015, No. 1, 714817, 2015.

[13] Naser, A. A., K. H. Sayidmarie, and J. S. Aziz, "Compact high isolation meandered-line PIFA antenna for LTE (band-class-13) handset applications," *Progress In Electromagnetics Research C*, Vol. 67, 153–164, 2016.

[14] Thummaluru, S. R. and R. K. Chaudhary, "Mu-negative metamaterial filter-based isolation technique for MIMO antennas," *Electronics Letters*, Vol. 53, No. 10, 644–646, 2017.

[15] Xue, C.-D., X. Y. Zhang, Y. F. Cao, Z. Hou, and C. F. Ding, "MIMO antenna using hybrid electric and magnetic coupling for isolation enhancement," *IEEE Transactions on Antennas and Propagation*, Vol. 65, No. 10, 5162–5170, 2017.

[16] Elfergani, I. T. E., J. Rodriguez, R. A. Abd-Alhameed, and I. Otung, "Dual-band MIMO balanced antenna for C-band and WLAN applications," in *The Loughborough Antennas & Propagation Conference (LAPC 2018)*, 1–6, Loughborough, Leicestershire, UK, 2018.

[17] Babu, K. V. and B. Anuradha, "Analysis of multi-band circle MIMO antenna design for C-band applications," *Progress In Electromagnetics Research C*, Vol. 91, 185–196, 2019.

[18] Kumar, A., A. Q. Ansari, B. K. Kanaujia, and J. Kishor, "A novel ITI-shaped isolation structure placed between two-port CPW-fed dual-band MIMO antenna for high isolation," *AEU — International Journal of Electronics and Communications*, Vol. 104, 35–43, 2019.

[19] Ameen, M., O. Ahmad, and R. K. Chaudhary, "Single split-ring resonator loaded self-decoupled dual-polarized MIMO antenna for mid-band 5G and C-band applications," *AEU — International Journal of Electronics and Communications*, Vol. 124, 153336, 2020.

[20] Ranjan, P., M. Patil, S. Chand, A. Ranjan, S. Singh, and A. Sharma, "Investigation on dual-port printed MIMO antenna with reduced RCS for C-band radar application," *International Journal of RF and Microwave Computer-Aided Engineering*, Vol. 30, No. 3, e22092, 2020.

[21] Sokunbi, O. and H. Attia, "Dual-layer dual-patch EBG structure for isolation enhancement and correlation reduction in MIMO antenna arrays," *Progress In Electromagnetics Research C*, Vol. 100, 233–245, 2020.

[22] Yang, Z., J. Xiao, and Q. Ye, "Enhancing MIMO antenna isolation characteristic by manipulating the propagation of surface wave," *IEEE Access*, Vol. 8, 115 572–115 581, 2020.

[23] Bhatia, S. S. and N. Sharma, "Modified spokes wheel shaped MIMO antenna system for multiband and future 5G applications: Design and measurement," *Progress In Electromagnetics Research C*, Vol. 117, 261–276, 2021.

[24] Islam, H., S. Das, T. Ali, P. Kumar, S. Dhar, and T. Bose, "Split ring resonator-based bandstop filter for improving isolation in compact MIMO antenna," *Sensors*, Vol. 21, No. 7, 2256, 2021.

[25] Chaudhary, A. K. and M. Manohar, "A modified SWB hexagonal fractal spatial diversity antenna with high isolation using meander line approach," *IEEE Access*, Vol. 10, 10 238–10 250, 2022.

[26] Nikam, P. B., J. Kumar, V. Sivanagaraju, and A. Baidya, "Dual-band reconfigurable EBG loaded circular patch MIMO antenna using defected ground structure (DGS) and PIN diode integrated branch-lines (BLs)," *Measurement*, Vol. 195, 111127, 2022.

[27] Arshad, M. A., M. Zahid, Y. Amin, and S. S. Jaffer, "MIMO antenna for C-band applications," in *2023 International Multidisciplinary Conference in Emerging Research Trends (IMCERT)*, Vol. 1, 1–5, Karachi, Pakistan, 2023.

[28] Sadineni, R. B. and P. Dinesha, "Design and development of a miniaturized highly isolated UWB-MIMO diversity antenna with quad band notch characteristics," *Progress In Electromagnetics Research C*, Vol. 131, 197–208, 2023.

[29] Chung, M.-A., C.-C. Hsu, and C. W. Yang, "Ring-opening 2×2 MIMO antenna for Sub-6G and WiFi-6E," in *2023 Asia-Pacific Microwave Conference (APMC)*, 215–218, Taipei, Taiwan, 2023.

[30] Wang, Z., W. Ren, W. Nie, W. Mu, and C. Li, "Design of three-band two-port MIMO antenna for 5G and future 6G applications based on fence-shaped decoupling structure," *Progress In Electromagnetics Research C*, Vol. 134, 249–261, 2023.

[31] You, X., C. Du, and Z.-P. Yang, "A flexible CPW 2-port dual notched-band UWB-MIMO antenna for wearable IoT applications," *Progress In Electromagnetics Research C*, Vol. 128, 155–168, 2023.

[32] Khedr, A. A., B. E. Elnaghi, and A. M. Mohamed, "Design of a compact dual port 2×1 ultra-wideband MIMO antenna for radio frequency energy harvesting based on four "a" shaped slots," *Progress In Electromagnetics Research M*, Vol. 128, 41–49, 2024.

[33] Kumar, P., A. K. Singh, R. Kumar, S. K. Mahto, P. Pal, R. Sinha, A. Choubey, and A. J. A. Al-Gburi, "Design and analysis of low profile stepped feedline with dual circular patch MIMO antenna and stub loaded partial ground plane for wireless applications," *Progress In Electromagnetics Research C*, Vol. 140, 135–144, 2024.

[34] Kumar, A., G. Singh, M. K. Abdulhameed, S. R. Hashim, and A. J. A. Al-Gburi, "Development of fractal 5G MIMO antenna for sub 6 GHz wireless automotive applications," *Progress In Electromagnetics Research M*, Vol. 130, 121–128, 2024.

[35] Song, Z., S. Zhao, S. Li, J. Chen, and Y. Xue, "High-isolation compact MIMO antenna with distributed metamaterial loading," *Progress In Electromagnetics Research M*, Vol. 128, 51–59, 2024.

[36] Tao, Y., H. Lin, M. Yang, W. Nie, C. Li, and M. Wang, "Sickle-shaped tri-band MIMO antenna for 5G and X-band applications," *Progress In Electromagnetics Research C*, Vol. 147, 15–25, 2024.

[37] Thakur, E., N. Jaglan, A. Gupta, and A. J. A. Al-Gburi, "Multi-band notched circular polarized MIMO antenna for ultra-wideband applications," *Progress In Electromagnetics Research M*, Vol. 125, 87–95, 2024.

[38] Wang, Z., G. Song, W. Nie, M. Yang, C. Li, and M. Wang, "A racket-like UWB MIMO antenna with high isolation," *Progress In Electromagnetics Research C*, Vol. 144, 159–168, 2024.

[39] Zhao, L., A. Li, Y. Wang, D. Song, M. Zheng, C. Liu, C. Li, Y. Liang, H. Zhao, and C. Hu, "Two-port hexagon-shaped MIMO antenna for UWB applications integrated with four frequently-used stopbands for medical domains," *Progress In Electromagnetics Research M*, Vol. 128, 145–153, 2024.

[40] Beigi, P., M. Rezvani, Y. Zehforoosh, J. Nourinia, and B. Heydarpanah, "A tiny EBG-based structure multiband MIMO antenna with high isolation for LTE/WLAN and C/X bands applications," *International Journal of RF and Microwave Computer-Aided Engineering*, Vol. 30, No. 3, e22104, 2020.

[41] Abdollahvand, M. and G. R. Dadashzadeh, "Compact double-fed dual annular ring printed monopole antenna for UWB application," *Journal of Electromagnetic Waves and Applications*, Vol. 23, No. 14-15, 1969–1980, 2009.

[42] Vaughan, R. G. and J. B. Andersen, "Antenna diversity in mobile communications," *IEEE Transactions on Vehicular Technology*, Vol. 36, No. 4, 149–172, 1987.

[43] Thaysen, J. and K. B. Jakobsen, "Envelope correlation in (N, N) MIMO antenna array from scattering parameters," *Microwave and Optical Technology Letters*, Vol. 48, No. 5, 832–834, 2006.

[44] Monebhurrun, V., S. Chakrabarti, and R. Quoi, "A 5G NR FR1 UWB antenna as benchmark for the development of IEEE Standard P2816," in *2023 Antenna Measurement Techniques Association Symposium (AMTA)*, 1–2, Renton, WA, USA, 2023.

[45] Monebhurrun, V., J. Fordham, L. Foged, and V. Rodriguez, "Application of IEEE Std 149–2021™: International antenna measurement campaign," in *2024 Antenna Measurement Techniques Association Symposium (AMTA)*, 1–2, Cincinnati, OH, USA, 2024.

[46] Ameen, M., O. Ahmad, and R. K. Chaudhary, "Wideband circularly-polarised high-gain diversity antenna loaded with metasurface reflector for small satellite applications," *Electronics Letters*, Vol. 55, No. 15, 829–831, 2019.

[47] Ameen, M. and R. K. Chaudhary, "Isolation enhancement of metamaterial-inspired two-port MIMO antenna using hybrid techniques," *IEEE Transactions on Circuits and Systems II: Express Briefs*, Vol. 70, No. 6, 1966–1970, 2023.

[48] Han, M.-S. and J. Choi, "Multiband MIMO antenna with a band stop filter for high isolation characteristics," in *2009 IEEE Antennas and Propagation Society International Symposium*, 1–4, North Charleston, SC, USA, 2009.

[49] Wan, Z., Y. He, Y. Bai, and H. Sun, "Compact, copolarized, and high-isolation two-port patch antenna for MIMO applications," *IEEE Antennas and Wireless Propagation Letters*, Vol. 22, No. 11, 2705–2709, 2023.